Hofmann et al. International Journal of Mechanical and Materials Engineering (2021) 16:9
https://doi.org/10.1186/s40712-021-00129-3

International Journal of Mechanical and Materials Engineering

ORIGINAL PAPER Open Access

Friction and contact temperature in dry rolling-sliding contacts with MoS_2-bonded and a-C:H:Zr DLC coatings

Stefan Hofmann*, Mustafa Yilmaz, Enzo Maier, Thomas Lohner and Karsten Stahl

Abstract

Gearboxes are usually lubricated with oil or grease to reduce friction and wear and to dissipate heat. However, gearbox applications that cannot be lubricated with oil or grease, for example in the space or food industry, are commonly lubricated with solid lubricants. Especially solid lubricants with a lamellar sliding mechanism like graphite and molybdenum disulfide (MoS_2) or diamond-like carbon (DLC) coatings can enable very low coefficients of friction. This study investigates the friction and temperature behavior of surface coatings in rolling-sliding contacts for the application in dry lubricated gears. In an experimental setup on a twin-disk test rig, case-hardened steel 16MnCr5E (AISI5115) is considered as substrate material together with an amorphous, hydrogenated, and metal-containing a-C:H:Zr DLC coating (ZrC_g) and a MoS_2-bonded coating (MoS_2-BoC). The friction curves show reduced coefficients of friction and a significantly increased operating area for both surface coatings. Due to the sufficient electrical insulation of the MoS_2-BoC, the application of thin-film temperature measurement-known from lubricated contacts-was successfully transfered to dry rolling-sliding contacts. The results of the contact temperature measurements reveal pronounced thermal insulation with MoS_2-BoC, which can interefere the sliding mechanism of MoS_2 by accelerated oxidation. The study shows that the application of dry lubricated gears under ambient air conditions is challenging as the tribological and thermal behavior requires tailored surface coatings.

Keywords: Solid lubricants, DLC, MoS_2, Dry lubrication, Thin film sensors

Introduction

Solid lubricants have become particularly important in the 1960s due to the space industry, since prevailing vacuum conditions obstruct the use of fluid lubrication. Nowadays, dry lubrication is generally also important in hygenic environments and in engineering designs with extreme lightweight or thermal requirements. It can present an ecological alternative to fluid lubricants in suitable applications. In gearboxes, dry lubrication omits the use of expensive seals and drastically reduces no-load power losses (Höhn et al. 2009).

Solid lubricants with a lamellar sliding mechanism like graphite, molybdenum disulfide (MoS_2), and tungsten disulfide (WS_2) have been shown to reduce friction and wear. However, the tribological performance strongly depends on the environmental conditions ((Gradt and Schneider 2016) and (Banerjee and Chattopadhyay 2014)) and the provision of the solid lubricants in the tribological system (Birkhofer and Kümmerle 2012). Investigations on the life time of dry lubricated bearings from (Schul 1997) show higher friction and wear of bonded compared to sputtered MoS_2 coatings. According to (Dienwiebel et al. 2004) and (Li et al. 2017), solid lubricants with lamellar sliding mechanism can reach the friction regime of superlubricity. (Hirano and Shinjo 1990) introduced this friction regime, which is attributed to coefficients of friction below $\mu \leq 0.01$. However, the

* Correspondence: s.hofmann@fzg.mw.tum.de
This paper is an extended version of an abstract published in the 61st German Tribology Conference, Göttingen, Germany, 28–30 September 2020.
Gear Research Centre (FZG), Technical University of Munich (TUM), Boltzmannstr. 15, 85748 Garching near Munich, Germany

requirements for achieving superlubricity are numerous and can only be observed on microscale (Berman et al. 2018). On a ball-on-disk tribometer under vacuum conditions, sputtered MoS_2 enabled coefficients of friction as low as 0.05 (Gradt and Schneider 2016). Investigations from (Gamyula et al. 1984) revealed coefficients of friction below 0.02 for MoS_2-bonded coating on a ball-on-disk tribometer. However, in contrast to graphite, significant relative humidity (RH) under ambient air conditions leads to an sharp increase in friction and wear for MoS_2 (Vazirisereshk et al. 2019). Metallic elements like chromium or titanium can be added to increase wear resistance, whereas there is no remarkable influence on frictional behavior according to (Banerjee and Chattopadhyay 2014) and (Gradt and Schneider 2016). Moreover, it is possible that high contact temperatures interfere with the sliding mechanism due to the oxidation of, e.g., MoS_2 to MoO_3, which leads to a structural change of the lattice-layer structure (Zhang et al. 2011). Investigations from (Xu et al. 2003) reveal to increased wear for a MoS_2-bonded coating at temperatures above 100 °C compared to room temperature, which was attributed to oxidation of MoS_2.

In addition to bonded coatings and pure solid lubricant layers, diamond-like carbon (DLC) coatings can also reduce friction and provide high wear resistance even at high loads. The mechanical and tribological properties of DLC coatings can be strongly influenced by the ratio of sp^2- to sp^3-bonded carbon, the hydrogen content and doping elements (Donnet and Erdemir 2008). Especially DLC coatings with high proportions of amorphous sp^2 carbon bonds and hydrogen (a-C:H) can result in ultra-low friction under dry lubrication. Investigations in high vacuum on a linear reciprocating pin-on-disk tribometer showed coefficients of friction as small as 0.005 for an a-C:H DLC coating (Fontaine et al. 2005). Also (Erdemir and Eryilmaz 2014) observed coefficients of friction in the range of 0.001 in a dry atmosphere on a ball-on-disk tribometer for a highly hydrogenated DLC coating. Such low coefficients of friction are attributed to superlubricity (Hirano and Shinjo 1990). However, the tribological properties of DLC coatings also depend strongly on environmental conditions, where the humidity of the ambient air plays a major role according to (Weihnacht et al. 2012) and (Schultrich and Weihnacht 2008). (Ronkainen et al. 1998) determined coefficients of friction of $0.15 < \mu < 0.22$ in ambient air with RH = 50 % on a pin-on-disk tribometer for a-C:H and a-C DLC coatings, which are similar to the results from (Donnet et al. 1994) at RH = 40 %. Investigations from (Yilmaz et al. 2018) on a twin-disk test rig under dry lubrication in ambient air showed coefficients of friction in the range of $0.10 < \mu < 0.18$ for a tetrahedral ta-C DLC coating.

(Grossl 2007) and (Martens 2008) conducted experimental investigations on a gear test rig under dry lubrication in ambient air and showed improved durability of ta-C DLC-coated gears. Uncoated gears demonstrated significant scuffing failure after a short running time. The durability can be further increased by low-loss gear designs (Hinterstoißer et al. 2019).

The aim of this study is the evaluation of operating limits and the characterization of friction and temperature behavior of two different surface coatings for reliable operation of dry lubricated rolling-sliding contacts. Besides an amorphous, hydrogenated, and metal-containing a-C:H:Zr (ZrC_g) DLC coating, a MoS_2-bonded coating (MoS_2-BoC) based on polyimide is used. As the focus is put on transferability of load and kinematic conditions to gears, a twin-disk test rig is used. Besides friction and bulk temperature, the contact temperature is measured for MoS_2-BoC using thin-film sensor technology in order to get insight into the shearing mechanism.

Experimental setup

The following sections describe the considered twin-disk test rig, the test disks for friction and contact temperature measurements, the operating conditions, and the thin-film sensor technology.

FZG twin-disk test rig

Figure 1 shows the mechanical layout of the considered FZG twin-disk test rig, which was designed by (Stößel 1971). The description and formulations are mainly adopted from (Lohner et al. 2015) and (Reitschuster et al. 2020). Both test disks are press-fitted onto shafts that can be driven independently by two three-phase motors. Traction drives mounted between the motors and driving shafts allow a continuous variation of speed. The normal force F_N in the disk contact is applied by a pneumatic cylinder via the pivot arm where the lower disk is mounted. The upper disk is mounted in a skid, which is attached to the frame by thin steel sheets. The skid is supported laterally by a load cell to ensure that the friction force F_R in the disk contact for sliding velocities $v_g \neq 0$ m/s can be measured as a reaction force with hardly any displacement of the skid. Normal force F_N, friction force F_R, surface velocities v_1 and v_2, and bulk temperature of the upper disk ϑ_M are measured. ϑ_M is recorded by a Pt100 resistance temperature sensor 5 mm below the surface of the disk. The coefficient of friction is calculated according to Eq. (1).

$$\mu = \frac{F_R}{F_N} \tag{1}$$

The sum velocity v_Σ is defined as the sum of the surface velocity of the upper disk v_1 and the surface velocity

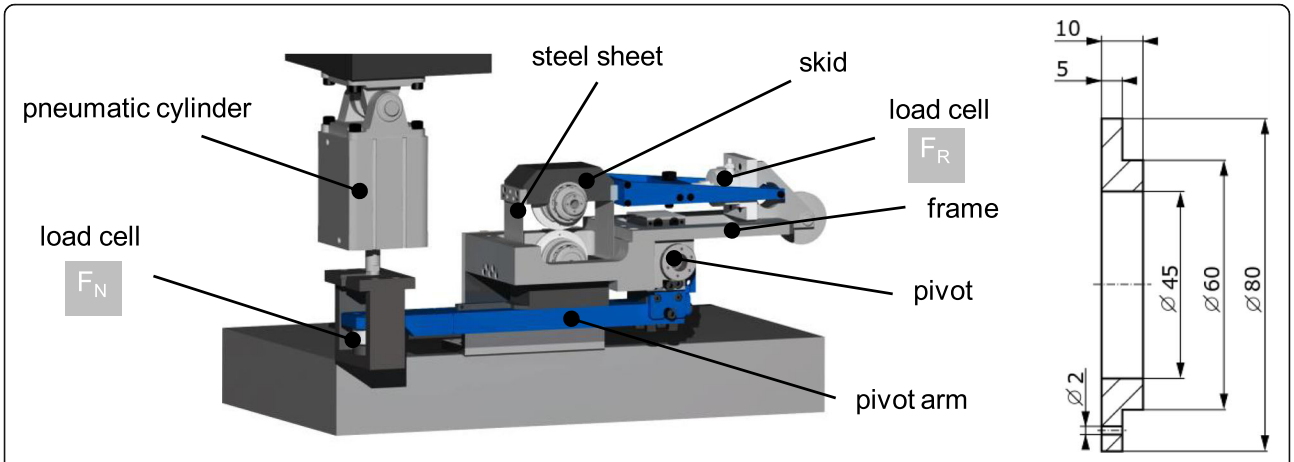

Fig. 1 Mechanical layout of the FZG twin-disk test rig and geometry of the test disks (Reitschuster et al. 2020)

of the lower disk v_2, whereas the sliding velocity v_g is defined as the difference between the surface velocities v_1 and v_2:

$$v_{\sum} = v_1 + v_2 \text{ with } v_1 > v_2 \tag{2}$$

$$v_g = v_1 - v_2 \tag{3}$$

The slip ratio s is defined as

$$s = \frac{v_1 - v_2}{v_1} \cdot 100\% \tag{4}$$

All experiments are carried out under line contact conditions with cylindrical disks having a diameter of 80 mm and a width of 5 mm according to Fig. 1.

Test disks

All test disks were made of case-hardened steel 16MnCr5E (AISI5115) with a surface hardness of 60 ± 2 HRC and a case hardening depth of CHD_{550HV1} = 0.9 ± 0.2 mm. The preparation of the running surface was adapted to each coating process. ZrC_g coated disks were peripherally ground and polished to an arithmetic mean roughness value Ra ≤ 0.01 μm to ensure high adhesion of the coating-bonding system. DLC coating graded zirconium carbide (ZrC_g) was deposited by middle frequency magnetron sputtering (mfMS) at the Surface Engineering Institute (IOT) RWTH Aachen University, Aachen, Germany. Thereby an industrial coating unit was used with two zirconium targets with a purity > 99.5 % and argon (Ar) and acethylene (C_2H_2) as process and reactive gas. To avoid annealing effects of the case-hardened steel, temperature during the physical vapor deposition (PVD) process was limited to 180 °C. Further process parameters can be found in (Bobzin et al. 2015). The coating possesses of a crystalline zirconium interlayer on steel substrate and a graded zirconium carbide layer with increasing portions of carbon. The maximum carbon ratio is reached at the zirconium and hydrogen containing top layer with an amorphous structure a-C:H:Zr. Young's modulus E = 110 ± 12 GPa is lower compared to the steel substrate with E = 210 GPa. Total film thickness was t_c = 3.2 μm. MoS_2-BoC for friction measurements was applied by spraying at FUCHS LUBRITECH GmbH, Kaiserslautern, Germany, and consists of solid lubricant particles dispersed in an organic binder matrix. In order to increase adhesion between lacquer and substrate, a surface roughness of Ra ≈ 0.5 μm after hardening was chosen before coating as recommended by (Gamyula et al. 1984) and (Yukhno et al. 2001) for bonded coatings. For the coating process, the disks were heated up to 100 °C, sprayed manually, and tempered in a convection oven for 1 h at 200 °C. A total coating thickness of t_c =15 ± 2 μm was measured with the magnetic induction test method according to DIN EN ISO 2178. For contact temperature measurements, a MoS_2-BoC was used that consists of 70 wt.% polyimide as binder and 30 wt.% of MoS_2 and was applied at INM Saarbrücken, Germany. An identical coating process was applied. The total coating thickness was t_c = 25 ± 5 μm. Figure 2 shows a representative uncoated, ZrC_g coated and MoS_2-BoC coated test disk before the test run. It can be seen that the optical appearance and roughness strongly depends on the preparation and coating method. The mfMS PVD coating technology leads to a slight increase in arithmetic roughness from Ra ≤ 0.01 μm to Ra = 0.03 μm, whereas MoS_2-BoC considers a slight increase from Ra ≈ 0.5 μm to Ra = 0.61 μm. The MoS_2 solid lubricant particles of MoS_2-BoC are visible due to the colored reflections of the light of the microscope.

All surface roughness measurements were performed in axial direction by a profile method according to DIN EN ISO 13565-1 to 13565-3 with a measured length of

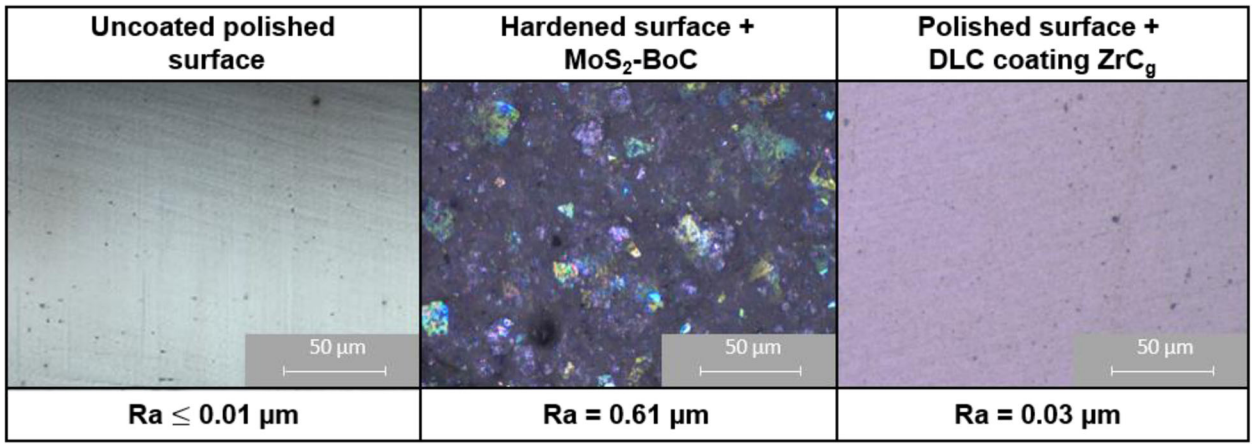

Fig. 2 Initial optical scans and mean arithmetic roughness of considered test disks

L_t = 4.0 mm and a cut-off wavelength of λ_c = 0.08 mm and 0.8 mm, respectively.

Thin-film sensors

Besides infrared technology, thin-film sensors enable high-resolution contact temperature measurements. With these, resistance measurements take advantage of the high sensitivity of a suitable sensor material to a change in temperature or pressure during the transit of the thin-film sensor through a tribological contact. Initial pressure measurements in elastohydrodynamic (EHL) contacts on a twin-disk test rig with manganin sensors started in the 1960s in investigations of (Kannel et al. 1965). Since then, numerous authors have carried out contact temperature and pressure measurements in elastohydrodynamic contacts on model test-rigs with thin-film sensor technology, e.g., (Schouten 1973), (Baumann 1987), (Bauerochs 1989), (Kagerer and Königer 1989), and (Mayer 2013). Measurements on gears and bearings can only be found from a few authors like (Kagerer 1991) and (Kühl 1996). Whereas the thin-film sensor technology is highly developed for lubricated contacts with high fluid load portions, measurements in dry lubricated contacts remain unexplored.

Within this study, thin-film sensors made of platinum were used for contact temperature measurements. The sensors were applied on zirconium dioxide (ZrO_2) disks to provide electrical insulation. A titanium adhesion layer with a thickness of approximate 40 nm on the ZrO_2 disks improved durability of the thin-film sensor. For both layers (titanium and platinum) ion beam sputtering was used. Figure 3 illustrates the considered sensor geometry, which has been successfully applied for EHL contact temperature measurements ((Kagerer 1991), (Mayer 2013), (Ebner et al. 2020)). The manufacturing process consists of masking with photolithography technique and sputtering of the titanium bonding layer and platinum sensor respectively. The sensor height of the thin film sensor is 100–150 nm, which results in an ohmic resistance value of $R_S \approx 120\ \Omega$. A detailed description of the manufacturing process can be found in (Ebner et al. 2020). The ohmic resistance of platinum shows high sensitivity to temperature and weak influence of pressure. The ratio between the temperature and pressure coefficient α_T and α_P is high, which results

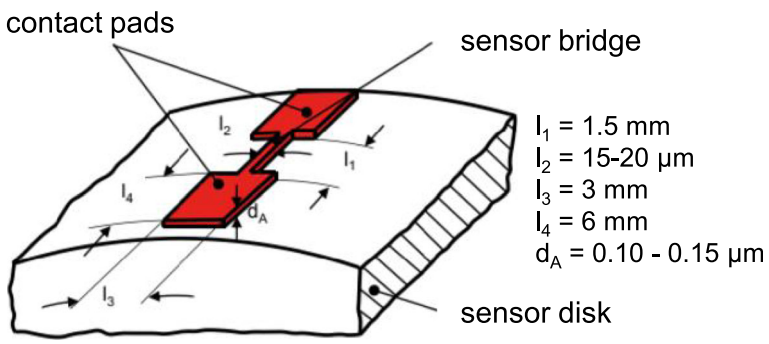

Fig. 3 Thin-film sensor geometry for contact temperature measurements (Ebner et al. 2020)

in high sensitivity of the measurand compared to the measuring method. Equation (5) shows the correlation of relative resistance change of platinum $\Delta R_{Pt}/\Delta R_{0,Pt}$ to temperature (ΔT) and pressure change (Δp).

$$\frac{\Delta R_{Pt}}{R_{0,Pt}} = \alpha_{p,Pt} \cdot \Delta p + \alpha_{T,Pt} \cdot \Delta T \tag{5}$$

During the transit of the thin-film sensor through the contact, temperature and pressure changes always occur simultaneously such that the pressure distribution has to be known to calculate the temperature rise ΔT. For the used platinum thin-film sensor, the temperature coefficient $\alpha_{T,\ Pt} = 1.16 \cdot 10^{-3}$ 1/K is two orders in magnitude higher than the pressure coefficient $\alpha_{p,\ Pt} = -1.10 \cdot 10^{-5}$ mm^2/N.

For evaluation of the influence of MoS_2-BoC on the contact temperature, Table 1 supplements the material data and thermophysical properties of steel, ZrO_2, and polyimide. The latter approximates the properties of the MoS_2-BoC. The thermal effusivity e represents the ability to transport heat by conduction and convection (also known as thermal inertia (Ziegltrum et al. 2020) and is defined by Eq. (6).

$$e = \sqrt{\rho \cdot c_P \cdot \lambda} \tag{6}$$

Thereby, ρ describes the density, c_p the specific heat capacity, and λ the thermal conductivity of the considered substrate or surface coating.

Operating conditions

Friction curves and bulk temperatures were measured for various operating conditions shown in Table 2. Each friction curve was recorded at a constant normal force of F_N = 435 N, which corresponds to a Hertzian pressure of p_H = 400 MPa for the contact of uncoated disks. For each considered sum velocity v_Σ, the slip ratio s was incrementally increased from s = 0 % to s = 50 %. All coefficients of friction μ and bulk temperatures ϑ_M were recorded in quasi-stationary states characterized by a bulk temperature change $\Delta\vartheta_M/\Delta t \leq 0.5$ K/min. After reaching the maximum slip ratio of s = 50 %, the system was left at rest to cool down to room temperature before adjusting the next sum velocity v_Σ. Besides dry lubrication, reference measurements under oil injection lubrication were conducted with reference ISO VG100 mineral oil with 4 % of sulfur-phosphorus extreme pressure (EP) additive (FVA3A, (Laukotka 2007)). The oil was injected at a temperature ϑ_{oil} = 40 °C. To avoid damage, all friction curve measurements were aborted if the coefficient of friction exceeded μ = 0.5, or if the measured bulk temperature exceeded ϑ_M = 160 °C. Disks with the same surface finish according to Fig. 2 were paired. Each friction curve was measured twice with a new set of disks. The room was conditioned to 20 °C and a relative humidity of RH = 40 – 50 %.

Contact temperature measurements were performed at constant sum velocity v_Σ = 2 m/s, but different loads and slip ratios s, as shown in Table 2. The considered normal forces were F_N = {251, 446} N, which correspond to Hertzian pressures of the uncoated contact of p_H = {300, 400} MPa. The slip ratio ranged from s = 0 % to s = 30 %. After adjusting each operating point, the disks were brought into contact at the considered normal force F_N for about three seconds and six roll-overs from the thin-film sensor were tracked with a digital oscilloscope. This procedure was repeated once to achieve a total of twelve signals for each operating point.

Results

This section presents the experimental results divided into friction curves and contact temperature measurements.

Friction curve measurements

Figure 4 shows the measured coefficients of friction μ and bulk temperatures ϑ_M over the slip ratio s for a normal force of F_N = 435 N and sum velocities v_Σ = {1, 2, 4} m/s. Both friction curves of the uncoated polished surface under dry lubrication show a degressive increase of the coefficient of friction for a sum velocity v_Σ = 1 m/s up to a slip ratio s = 20%. A higher slip ratio results in a rapid increase in the coefficient of friction. Thus, the tests were aborted and a stationary value could not be measured. The results correspond to investigations by (Ebner et al. 2018) and (Yilmaz et al. 2018) for uncoated surfaces under dry lubrication. Measured bulk temperatures increase only slightly with increasing slip ratio for

Table 1 Material data and thermophysical properties (Benford et al. 1999), (Detakta 2015), (Deutsche Edelstahlwerke GmbH 2011), (Oxidkeramik J Cardenas GmbH 2015) (MoS_2-BoC values approximated by plain polyimide)

Material	Young's modulus E in N/mm^2	Poisson ratio ν	Density ρ in kg/m^3	Thermal conductivity λ in W/(mK)	Specific heat capacity c_p in J/(kgK)	Thermal effusivity e in $J/(K\sqrt{s}\ m^2)$
Steel	210,000	0.30	7760	44.00	431	12131
ZrO_2	200,000	0.30	6000	2.50	400	2449
Polyimide*	3000	0.34	1400	0.15	1090	486

Table 2 Operating conditions of friction and contact temperature measurements. Hertzian pressure calculated for the uncoated system

	Normal load F_N in N	Hertzian pressure p_H in MPa*	Sum velocity v_Σ in m/s	Slip ratio s in %
Friction curve measurements	435	400	1, 2, 4	0, 2, 5, 10, 20, 30, 40, 50
Contact temperature measurements	251, 446	300, 400	2	0, 10, 20, 30

the uncoated surface, even after the coefficient of friction had increased rapidly. Compared to the uncoated polished surfaces, MoS_2-BoC demonstrates a significantly increased operating area. The friction curves of MoS_2-BoC at v_Σ = 1 m/s show a similar profile as with the uncoated polished surface, but decrease at high slip ratios s > 30 %. For sum velocities v_Σ = {2, 4} m/s, both friction curves increase rapidly at small slip ratios and then decrease slightly with increasing slip ratio. The decrease of the coefficient of friction with increasing slip ratio can be referred to the lattice-layer structure of MoS_2 (Vazirisereshk et al. 2019). Corresponding bulk temperatures increase with increasing sum velocity and slip ratio due to rising frictional power in the disk contact. The first test run is aborted due to high friction force at a sum velocity v_Σ = 4 m/s and a slip ratio s = 50 %, the second test run did not reach the abortion criteria. The friction curves for DLC coating ZrC_g reveal frictional behavior similar to MoS_2-BoC. For a sum velocity v_Σ = 1 m/s, a sharp increase of the coefficient of

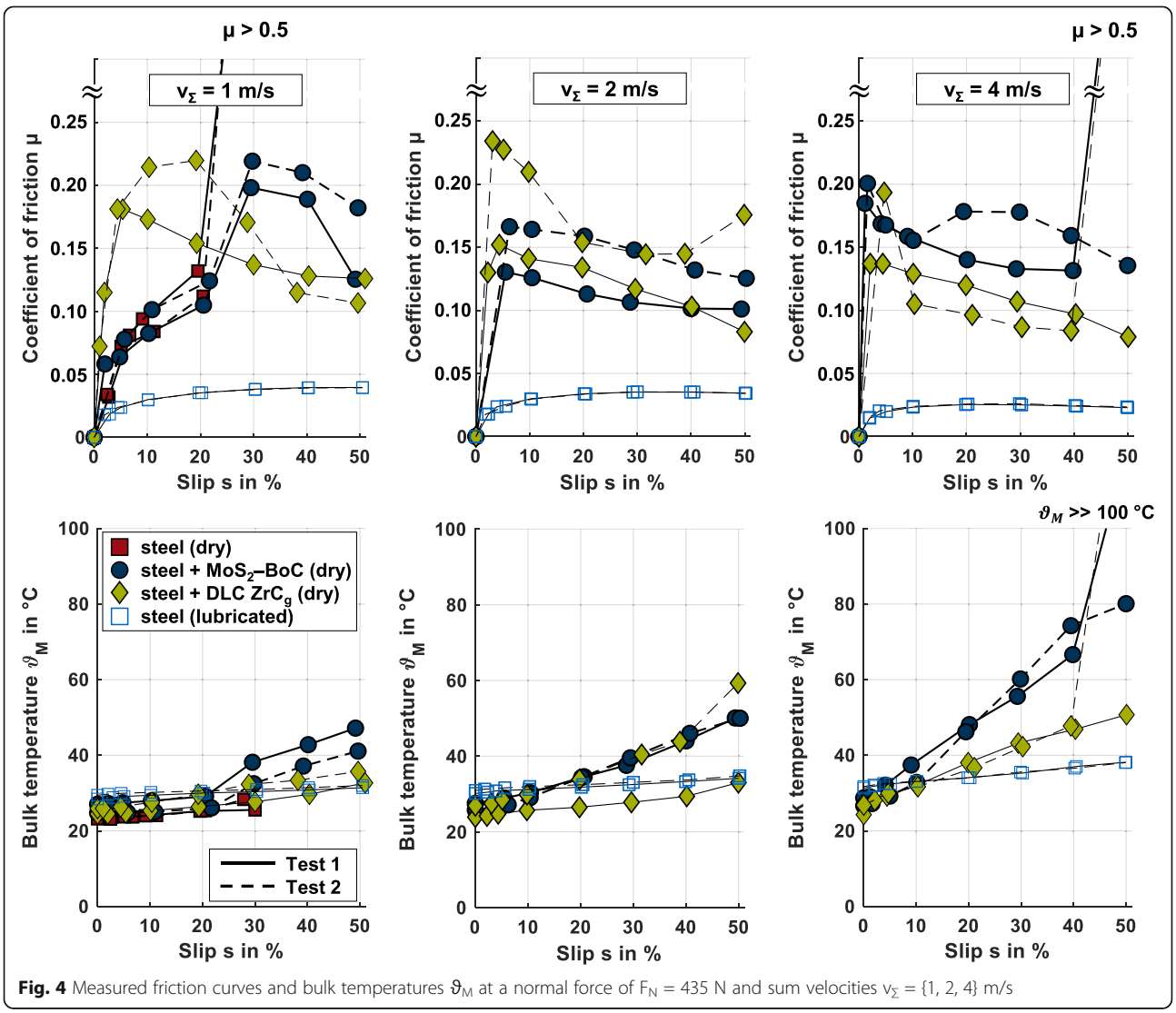

Fig. 4 Measured friction curves and bulk temperatures ϑ_M at a normal force of F_N = 435 N and sum velocities v_Σ = {1, 2, 4} m/s

friction up to a slip ratio s = 5 % and a moderate decrease for higher slip ratios is observed for the first test run. The second test run shows its maximum coefficient of friction at a slip ratio s = 20 % before it decreases to a similar level as the first test run. At higher sum velocities, the profile of the friction curves reveals a sharp increase to a maximum coefficient of friction at a slip ratio of s = 2 and 5 %, after which a continuous decrease occurs. The decrease of the coefficient of friction with an increasing slip ratio can be attributed to a temperature-induced structural transformation from carbon to graphite (Durst 2008) resulting in a lattice-layer structure. This transformation process is also observed in investigations on the frictional behavior of ta-C coatings by (Yilmaz et al. 2018). The corresponding bulk temperatures increase with increasing sum velocity and slip ratio due to rising frictional power in the contact. The second test run is aborted due to high friction force at a sum velocity v_Σ = 4 m/s and a slip ratio s = 50%.

The experimental results under oil injection lubrication with uncoated polished surfaces show significantly lower coefficients of friction and bulk temperatures. Despite the oil injection temperature of ϑ_{oil} = 40 °C, the bulk temperatures are lower for every operating condition due to heat convection into the surroundings. Compared to lubricated contacts, dry lubrication shows lower repetition accuracy and higher sensitivity to changes of the operating conditions, as seen in Fig. 4.

Figure 5 shows optical scans and corresponding mean arithmetic roughness Ra of all investigated surfaces under dry lubrication after the second test run. Note that the abortion limit was reached for the uncoated surface and DLC coating ZrC_g, which indicates that the operation area was exceeded, resulting in damage to the investigated surface. Despite the rise in surface roughness Ra, the uncoated surface shows brown discoloration, which may indicate oxidation processes. Similar observations by (Yilmaz et al. 2018) revealed the formation of Fe_2O_3 on the uncoated steel running surface under dry lubrication through energy-dispersive X-ray spectroscopy (EDX) element analysis. Generally, high friction is associated with tremendous local temperature developments that can lead to accelerated oxidation processes. MoS_2-BoC reveals a partial detachment of the bonded coating as the steel substrate becomes visible, whereas the surface roughness increases slightly to Ra = 1.01 µm. Clear changes can be observed for DLC coating ZrC_g in the optical appearance and increase of surface roughness to Ra = 3.18 µm.

Contact temperature measurements

Measurements of contact temperatures were considered for MoS_2-BoC. The polyimide matrix and solid lubricant particles are sufficient electrical insulators to not cause a short circuit between the contact pads of the thin-film sensor. Besides, MoS_2-BoC is soft compared to the platinum of the thin-film sensor, which inhibits detachment of the sensor from the sensor disk. Figure 6 shows the contact temperature rise ΔT^* above bulk temperature over the dimensionless gap length direction x/b_H for MoS_2-BoC at normal forces F_N = {251, 446} N, sum velocity v_Σ = 2 m/s and slip ratios s = {0, 10, 20, 30} %. Thereby, the dimensionless gap length direction represents the sensor distance × normalized by the half Hertzian contact width b_H in entraintment direction to enable a simpler visualization of different loads. All illustrated temperature profiles represent the mean value of up to twelve roll-overs. The signal scattering for F_N = 251 N is less than 1.2 K at a slip ratio s = 20 %. For slip ratios of s = {0, 10} %, the temperature scatters between 0.1 K and 0.2 K. At a normal force of F_N = 446 N, the scattering increases to a maximum of 6 K for a slip ratio of s = 30 %. The influence of pressure on the temperature profile was neglected (symbolized by *

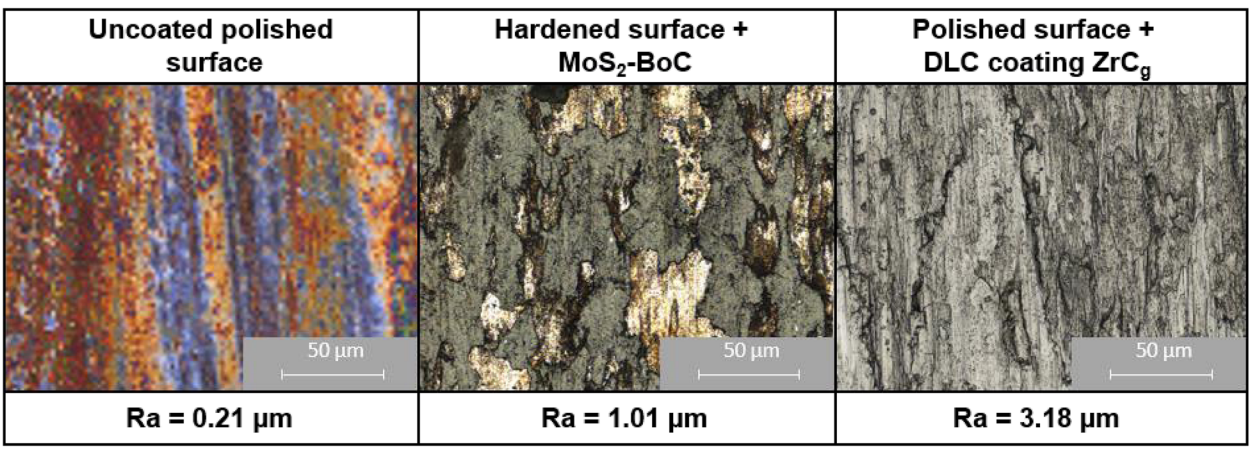

Fig. 5 Optical scans and mean arithmetic roughness Ra of test disks after the second test run

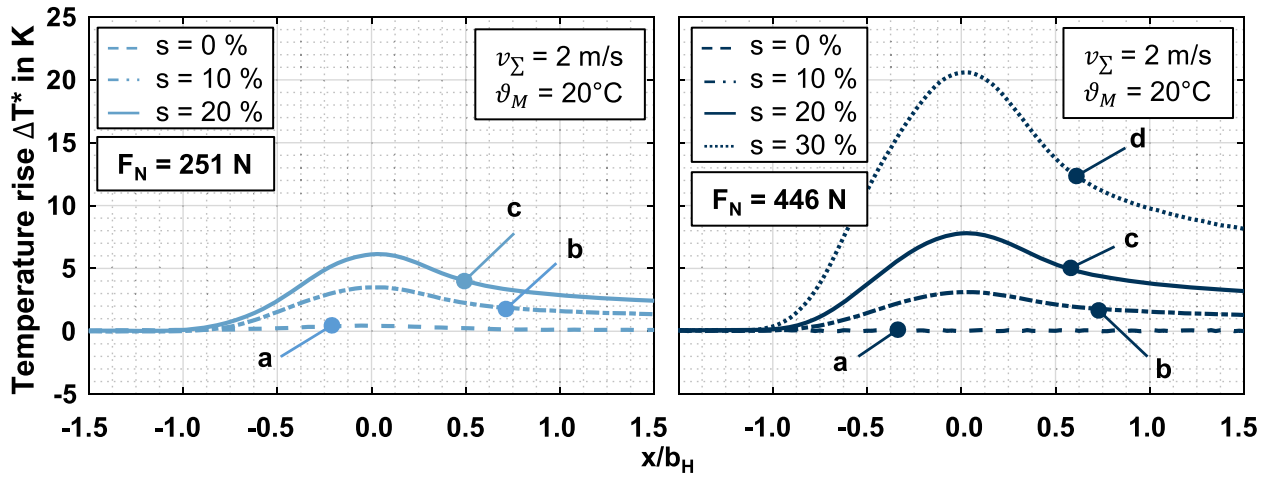

Fig. 6 Contact temperature rise ΔT* for normal forces F_N = {251, 446} N and slip ratios s = {0, 10, 20, 30} % for MoS_2-BoC

added to ΔT), which leads to underestimated temperature rises due to the negative pressure coefficient of platinum. As MoS_2-BoC with coating thickness t_c = 25 ± 5 µm affects contact pressure, a pressure correction based on p_H for the uncoated disk contact cannot be easily applied. Investigations by (Elsharkawy et al. 2006) on the influence of coatings Young's modulus and thickness on pressure distribution reveal significant lower maximum contact pressures for soft coatings. For a ratio of Young's moduli between substrate (E_s) and coating (E_c), E_s/E_c = 20, and a coating thickness of 20 µm, the maximum contact pressure can be as low as half the value of the uncoated system. However, since no detailed simulations are available for the considered MoS_2-BoC, no pressure correction was applied. The comparison of measured contact temperatures ΔT* is limited to the same normal force, although the maximum temperature change due to pressure is estimated to be small as the platinum sensor is much more sensitive to temperature as described in "Thin-film sensors" section.

At a normal load of F_N = 251 N, a maximum temperature rise ΔT^*_{max} = 0.5 K for pure rolling (curve a) was measured. This can be referred to hysteresis friction in the polyimide matrix and microslip. The temperature rise increases from ΔT^*_{max} = 3.5 K (curve b) up to ΔT^*_{max} = 6.2 K (curve c) for the highest investigated slip ratio s = 20 %. This can be referred to the increased sliding speed and hence friction power. Note that the coefficient of friction also increases slightly from µ = 0.046 (curve b) to µ = 0.054 (curve c). A similar pattern is observed at a normal load F_N = 446 N. The temperature rise ΔT^* also rises steadily with increasing slip ratio s. For pure rolling (curve a), the temperature rise is very small. For curve b, the temperature rise is ΔT^*_{max} = 3.1 K and for curve c, ΔT^*_{max} = 8.0 K. The maximum temperature rise ΔT^*_{max} = 20.5 K is observed for curve d at s = 30 %. As for the lower normal force, the coefficient of friction increases slightly from curve b to d, from µ = 0.040 to µ = 0.050 to µ = 0.051.

Discussion

In the following section, the experimental results are discussed with focus on the tribological behavior and thermal performance of the considered surface coatings.

Tribological performance of surface coatings

The experimental results in "Friction curve measurements" section under dry lubrication demonstrate a reduction of friction and an increase of the operating area by the considered surface coatings MoS_2-BoC and DLC coating ZrC_g compared to plain steel contacts. At higher sum velocities v_Σ, an increase in the slip ratio s can result in reduced friction. The measured coefficients of friction between 0.1 < µ < 0.2 for DLC coating ZrC_g correlate with the results from (Erdemir and Eryilmaz 2014) for an a-C:H DLC coating under ambient air conditions. The decrease in friction at higher slip ratio and sum velocities can be referred to the graphitization of amorphous carbon coatings. (Liu et al. 1996) conducted experiments on a pin-on-disk tribometer with similar load and sliding speeds as for the friction curves in Fig. 4 and observed a significant reduction of friction especially for high sliding. According to (Durst 2008), the graphitization starts from 300 °C, which can occur locally at asperity contacts with high local pressures and flash temperatures. Also for the MoS_2-BoC, the coefficients of friction are in agreement to further investigations. (Xu et al. 2003) performed experiments under ambient air conditions on a ball-on-disk tribometer with MoS_2-BoC and epoxy resin as binder. For a relative

humidity of RH = 50 % and room temperature (23 °C), coefficients of friction between 0.1 < μ < 0.2 were measured.

The coefficients of friction for contact temperature measurements in the "Contact temperature measurements" section are significantly lower than observed during friction curve measurements with MoS_2-BoC in the "Friction curve measurements" section. Although the comparison is restricted with respect to different disk pairings, testing time has to be considered. While the contact temperature measurements lasted only a few seconds, the total running time for a friction curve measurement can be up to 2 h. (Gradt and Schneider 2016) observed continuously increasing coefficients of friction over running time for MoS_2 coatings on a ball-on-disk tribometer. The results of friction curve measurements may indicate this behavior, since low coefficients of friction as low as μ = 0.05 to 0.1 were observed only for low slip ratios at a sum velocity of v_Σ = 1 m/s. For the sum velocity v_Σ = 1 m/s and the slip ratio s = 10 %, the measured coefficient of friction is μ = 0.09, whereas for the same sliding speed v_g at a sum velocity of v_Σ = 2 m/s (s = 5%), the measured mean coefficient of friction is μ = 0.15. This indicates that ongoing interaction in the contact accompanied with wear in the contact zone interferes with the sliding mechanism of the MoS_2-BoC. Note that also the bulk temperatures were higher during friction curve measurements, which may have an influence on the material properties of the polyimide binder matrix of the MoS_2-BoC. Investigations from (Tsai et al. 2003) on the temperature dependency of vapor deposited polyimide reveal a linear decrease in Young's modulus with increasing temperature. Hence, the increasing bulk temperatures for higher sum velocities and slip ratios may affect the tribological performance significantly.

The recorded coefficients of friction during contact temperature measurements in the "Contact temperature measurements" section also show a decrease with higher load as known for solid lubricants with a lamellar sliding mechanism (Gustavsson et al. 2013). According to (Donnet and Erdemir 2008) and (Kazuhisa 2001), coefficients of friction for compounds with lamellar sliding mechanism correlate to the contact area and shear stresses between the sliding planes. However, there is no linear relationship between load and contact area resulting in decreasing coefficients of friction for higher loads as observed by (Gradt and Schneider 2016) and (Gustavsson et al. 2013).

Thermal performance of surface coatings

The investigations with dry lubrication show significantly higher coefficients of friction than the investigations with oil injection lubrication. This higher friction power accompanied with a poor heat dissipation results in higher bulk temperatures. The related higher level of contact temperatures under dry lubrication are amplified by thermal insulation effects observed by contact temperature measurements with MoS_2-BoC.

To consider the influence of the thermophysical properties of MoS_2-BoC (see Table 1) on contact temperature, the flash temperatures T_{Bl} according to Blok (Blok 1937) are calculated by Eq. (7) for the material pairings ZrO_2/steel and ZrO_2/polyimide. Thereby, polyimide approximates the thermophysical properties of MoS_2-BoC. F_N represents the normal load, l_{eff} the width of the contact, E´ the reduced modulus, an R the radius of relative curvature. Index 1 refers to the upper disk (ZrO_2) and index 2 to the lower disk (steel or polyimide).

$$T_{Bl} = \frac{0.62 \cdot \mu \cdot \left(\frac{F_N}{l_{eff}}\right)^{0.75} \cdot \left(\frac{E'}{R}\right)^{0.25} \cdot |v_g|}{\sqrt{\lambda_1 \cdot \rho_1 \cdot c_{p,1} \cdot v_1} + \sqrt{\lambda_2 \cdot \rho_2 \cdot c_{p,2} \cdot v_2}} \tag{7}$$

As the temperature penetration depth is in the range of only a few micrometer (Habchi 2014) and (Ziegltrum et al. 2020), the influence of the steel substrate on the flash temperature can be neglected. T_{Bl} refers to the maximum contact temperature rise above bulk temperature and can thus be compared to the maximum temperature rise ΔT_{max} measured for MoS_2-BoC.

Figure 7 shows the maximum temperature rise ΔT_{max} measured for ZrO_2/MoS_2-BoC and the flash temperatures T_{Bl} calculated for ZrO_2/polyimide and ZrO_2/steel.

The comparison between the measured and calculated values for ZrO_2/MoS_2-BoC and ZrO_2/polyimide agree, with largest deviations at the slip ratio of s = 30 % at F_N = 446 N. The calculated flash temperatures for ZrO_2/steel are clearly lower than for the measured and calculated pair with the considered coating. This clearly indicates thermal insulation effects that are mainly caused by the low thermal effusivity of e = 486 J/(K$\sqrt{s}$m^2) of the MoS_2-BoC compared to steel with e = 12130 J/(K$\sqrt{s}$m^2). Numerical simulations of Ziegltrum et al. (Ziegltrum et al. 2020) reveal thermal insulation effects in lubricated steel/polymer contacts due to low thermal effusivity of polymers. Hence, especially the high proportions of polyimide binder matrix with its very low thermal conductivity (Benford et al. 1999) favors thermal insulation by MoS_2-BoC, since the thermal conductivity of MoS_2 is only slightly lower compared to steel (Peng et al. 2016). Thermal insulation has also been observed with coatings under oil lubrication (e.g. (Björling et al. 2014) and (Ebner et al. 2020)). Thereby, in contrast to dry lubricated contacts, thermal insulation can result in a reduction in the coefficient of friction, as the contact viscosity is reduced by high contact temperatures. It should be

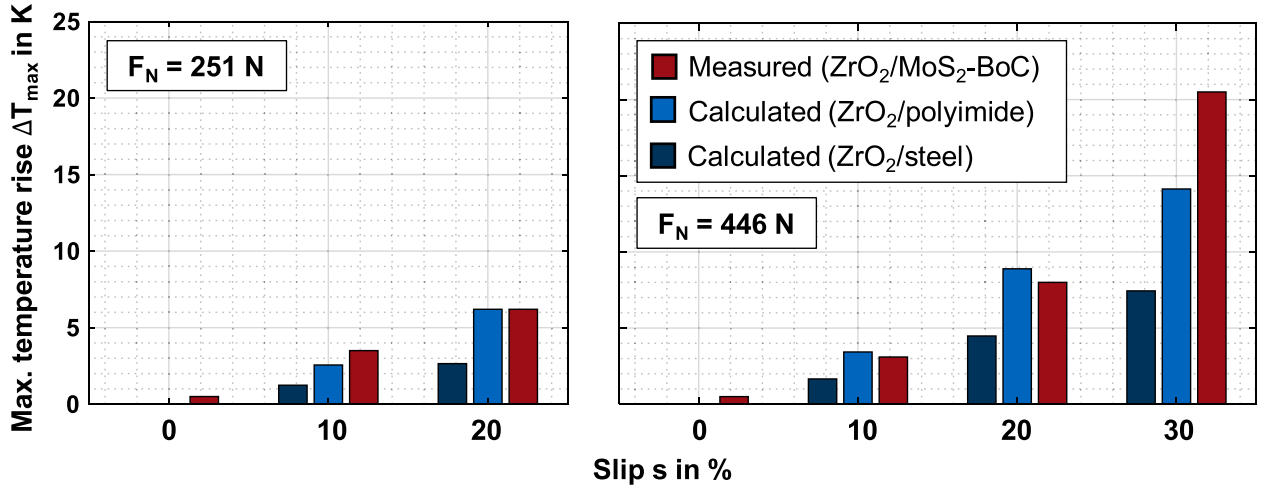

Fig. 7 Measured maximum relative temperature rise ΔT_{max} under dry lubrication at F_N = {251,446} N and v_Σ = 2 m/s and calculated flash temperatures

noted that the absolute contact temperatures measured with MoS_2-BoC are low in comparison for the considered operating conditions. This is mainly because the disks are in contact for approximately only twelve rollovers per operating point in order to avoid detachment and high wear of the platinum thin-film sensor. Hence, the measured bulk temperature is not quasi-stationary like for the friction curve measurements.

Nevertheless, the observed thermal insulation with high contact temperature rises can affect the performance of MoS_2-BoC since MoS_2 is sensitive to oxidation processes (Zhang et al. 2011). Investigations from (Xu et al. 2003) show significantly increased wear at temperatures above 100 °C for MoS_2-bonded coatings. Besides accelerated oxidation, high temperature levels can also result in reduced Young's modulus of the polymer binder matrix (Tsai et al. 2003). For DLC coatings, high contact temperatures can result in increased tribological performance as a structural change (graphitization) from sp^3- to sp^2-bonded carbon can occur.

It should be noted that no pressure correction was considered for the measured contact temperatures. For this and a detailed interpretation, numerical modelling can be applied to obtain the pressure and temperature distributions. In addition, the influence of the MoS_2 particles on the thermophysical properties of MoS_2-BoC should be investigated, whereby the thermal conductivity of filled polymers can show an anisotropic behavior (Mamunya et al. 2002).

Conclusion

This study investigated the friction and temperature behavior of rolling-sliding contacts under dry lubrication. Two surface coatings with different coating technologies were considered on a twin-disk test rig. To classify the results, uncoated polished surfaces were tested under dry and oil injection lubrication. The main conclusions of this study with respect to rolling-sliding contacts add

- The bearable load level of uncoated steel surfaces under dry lubrication is very low.
- Surface coatings can significantly increase operating areas under dry lubrication.
- Friction and bulk temperatures are considerably higher compared to oil lubrication.
- Contact temperatures under dry lubrication can be measured by thin-film sensors for bonded coatings if the electrical insulation is sufficient.
- Low thermal effusivity of bonded coatings can result in thermal insulation effects that can accelerate oxidation processes.

This study demonstrates the challenge of reliable implementation of e.g. gears with rolling-sliding contacts under dry lubrication under ambient air conditions. Nevertheless, the potential of tailored surface coatings under dry lubrication becomes clear. The lubrication and failure mechanisms have to be investigated further.

Abbreviations

MoS_2: Molybdenum disulfide; DLC: Diamond-like carbon; MoS_2-BoC: MoS_2-bonded coating; WS_2: Tungsten disulfide; RH: Relative humidity; EHL: Elastohydrodynamic lubrication; PVD: Physical vapor deposition; ZrO_2: Zirconium dioxide

Acknowledgements

N.A.

Authors' contributions

SH designed the experiments, analyzed the results, and wrote the paper with the support of MY. EM and TL supported the interpretation of the results, participated in the scientific discussions, and revised the paper. KS proofread the paper. All authors have read and agreed to the published version of the manuscript.

Funding
The presented results are based on the research project STA 1198/17-1 of the priority program SPP2074, supported by the German Research Foundation e.V. (DFG). The authors would like to thank for the sponsorship and support received from the DFG. Open Access funding was enabled and organized by Projekt DEAL.

Availability of data and materials
Data generated or analyzed during this study are included in this published article.

Declarations

Competing interests
The authors declare that they have no competing interests.

Received: 19 February 2021 Accepted: 18 May 2021
Published online: 15 June 2021

References

Banerjee, T., & Chattopadhyay, A. K. (2014). Structural, mechanical and tribological properties of pulsed DC magnetron sputtered TiN-WSx/TiN bilayer coating. *Surface & Coatings Technology*, 258;849–860.

Bauerochs, R. (1989). *Pressure- and temperature measurements in EHL rolling-sliding contacts (in German)*. Dissertation, Universität Hannover

Baumann, H. (1987). Measuring surface temperatures between rolling steel cylinders using double layer transducers. *Journal of Mechanical Engeneering Science*, *201*(4), 263–270. https://doi.org/10.1243/PIME_PROC_1987_201_119_02.

Benford, D. J., Power, T. J., & Moseley, S. H. (1999). Thermal conductivity of Kapton tape. *Cyrogenics*, *39*(1), 93–95. https://doi.org/10.1016/S0011-2275(98)00125-8.

Berman, D., Erdemir, A., & Sumant, A. V. (2018). Approaches for achieving superlubricity in two-dimension materials. *ACS Nano*, *12*(3), 2122–2137. https://doi.org/10.1021/acsnano.7b09046.

Birkhofer, H., & Kümmerle, T. (2012). *Feststoffgeschmierte Wälzlager: Einsatz, Grundlagen und Auslegung*. Berlin Heidelberg: Springer Vieweg. https://doi.org/10.1007/978-3-642-16797-3.

Björling, M., Larsson, R., & Marklund, P. (2014). The effect of DLC coating thickness on elastohydrodynamic friction. *Tribology Letters*, *55*(2), 353–362. https://doi.org/10.1007/s11249-014-0364-6.

Blok, H. (1937). *Theoretical study of temperature rise at surface of actual contact under oiliness lubrication*, *Proc. Gen. Disc. Lubric* (pp. 225–235). London: IME.

Bobzin, K., Brögelmann, T., Stahl, K., Michaelis, K., Mayer, J., & Hinterstoißer, M. (2015). Friction reduction of highly-loaded rolling-sliding contacts by surface modifications under elasto-hydrodynamic lubrication. *Wear*, 328-329,217–228.

Detakta (2015). *Material data sheet of Kapton HN-Polyimid Folie*. https://www.detakta.de/fileadmin/datenblaetter/flexiblelsolierstoffe/Kapton.pdf. Accessed 18 Aug 2020

Deutsche Edelstahlwerke GmbH (2011). *Material data sheet of 1.7131/1.7139 (16MnCr5/16MnCrS5)*. Witten. https://www.dew-stahl.com/fileadmin/files/dew-stahl.com/documents/Publikationen/Werkstoffdatenblaetter/Baustahl/1.7131_1.7139_de.pdf. Accessed 12 Dec 2018

Dienwiebel, M., Verhoeven, G. S., Pradeep, N., Frenken, J. W. M., Heimberg, J. A., & Zandbergen, H. W. (2004). Superlubricity of graphite. *Physical Review Letters*, *92*, 126101.

Donnet, C., Belin, M., Auge, J. C., Martin, J. M., Grill, A., & Patel, V. (1994). Tribochemistry of diamond-like carbon coatings in various enviroments. *Surface & Coatings Technology*, *68-69*, 626–631. https://doi.org/10.1016/0257-8972(94)90228-3.

Donnet, C., & Erdemir, A. (2008). *Tribology of diamond-like-carbon films: fundamentals and applications*. New York: Springer. https://doi.org/10.1007/978-0-387-49891-1.

Durst, O. (2008). *Corrosion and wear properties of new carbon-containing PVD layers (in German)*. Dissertation, Technische Universität Darmstadt

Ebner, M., Yilmaz, M., Lohner, T., Michaelis, K., Höhn, B.-R., & Stahl, K. (2018). On the effect of starved lubrication on elastohydrodynamic (EHL) line contacts. *Tribology International*, *118*, 515–523.

Ebner, M., Ziegltrum, A., Lohner, T., Michaelis, K., & Stahl, K. (2020). Measurement of EHL temperature by thin film sensors-Thermal insulation effects. *Tribology International*, *149*, 105515. https://doi.org/10.1016/j.triboint.2018.12.015.

Elsharkawy, A. A., Holmes, M. J. A., Evans, H. P., & Snidle, R. W. (2006). Micro-elastohydrodynamic lubrication of coated cylinders using coupled differential defletection method. *Proceedings of the Institution of Mechanical Engineers, Part J. Journal of Engineering Tribology*, 220,29–41.

Erdemir, A., & Eryilmaz, O. (2014). Achieving superlubricity in DLC films by controlling bulk, surface and tribochemistry. *Friction*, *2*(2), 140–155. https://doi.org/10.1007/s40544-014-0055-1.

Fontaine, J., Mogne, T., Loubet, J. L., & Belin, M. (2005). Achieving superlow friction with hydrogenated amorphous carbon: some key requirements. *Thin Solid Films*, *482*, 99–108.

Gamyula, G., Dobrovolskaya, G. V., Lebedeva, I. L., & Yukhno, T. P. (1984). *General regularities of wear in vacuum for solid film lubricant formulated with lamellar materials*.

Gradt, T., & Schneider, T. (2016). Tribological Performance of MoS2 Coatings in various Environments. *Lubricants*, *4*, 32.

Grossl, A. (2007). *Influence of PVD-coatings on the flank load carrying capacity and bending strenght of case hardened spur gears (in German)*. Dissertation, Technische Universität München

Gustavsson, F., Svahn, F., Bexell, U., & Jacobson, S. (2013). Nanoparticle based and sputtered WS2 low friction coatings - Differences and similarities with respect to friction mechanism and tribofilm formation. *Surface & Coatings Technology*, *232*, 616–626.

Habchi, W. (2014). A numerical model of the solution of thermal elastohydrodynamic lubrication in coated circular contacts. *Tribology International*, *73*, 57.

Hinterstoißer, M., Sedlmaier, M., Lohner, T., & Stahl, K. (2019). Minimizing load-dependent gear losses. *Tribologie und Schmierungstechnik*, *66*, 15–25.

Hirano, M., & Shinjo, K. (1990). Atomistic locking and friction. *Physical Review B*, *41*, 11837–11851.

Höhn, B.-R., Michaelis, K., & Otto, H.-P. (2009). Minimised gear lubrication by a minimum oil/air flow rate. *Wear*, *266*, 461–467.

Kagerer, E. (1991). *Measurement of elastohydrodynamic paramters in highly-loaded disk- and gear contacts (in German)*. Dissertation, Technische Universität München

Kagerer, E., & Königer, M. E. (1989). Ion beam sputter deposition of thin film sensors for applications in highly loaded contacts. *Thin Solid Films*, *182*, 333–344.

Kannel, J., Bell, J. C., & Allen, C. M. (1965). Methods for determining pressure distributions between lubricated rolling contacts. *ASLE Transactions*, 8,250–270.

Kazuhisa, M. (2001). *Solid Lubricants-Fundamental and applications*. Washington: Marcel Dekker Inc.

Kühl, S. (1996). *Joint contact resolved measurement of pressure and temperature in the elastohydrodynamic line contact of force-transmitting involute gears (in German)*. Dissertation, Technische Universität Clausthal

Laukotka, E. (2007). *FVA-Reference oil catalog-Reference oil data sheet. FVA Heft 660*. Frankfurt/Main: Forschungsvereinigung Antrieb e. V (in German).

Li, H., Wang, J., Gao, S., Chen, Q., Peng, L., Liu, K., & Wei, X. (2017). Superlubricity between MoS2 monolayers. *Advanced Materials*. 29(27),1701474.

Liu, Y., Erdemir, A., & Meletis, E. I. (1996). An investigation of the relationship between graphitization and fricitonal behavior of DLC coatings. *Surface & Coatings Technology*, *86-87*, 564–568. https://doi.org/10.1016/S0257-8972(96)03057-5.

Lohner, T., Merz, R., Mayer, J., Michaelis, K., Kopnarski, M., & Stahl, K. (2015). On the effect of plastic deformation (PD) additives in lubricants. *Tribologie und Schmierungstechnik*, 62(2),13–24.

Mamunya, Y. P., Davydenko, V. V., Pissis, P., & Lebedev, E. V. (2002, 1887–1897). Electrical and thermal conductivity of polymers filled with metal powders. *European Polymer Journal*, *38*.

Martens, S. (2008). *Oilfree industrial transmissions - Measures and possibilities to minimize or eliminate conventional lubricants (in German)*. Dissertation, Technische Universität Dresden

Mayer, J. (2013). *Influence of the surface and lubricant on the frictional behavior in EHL contact (in German)*. Dissertation, Technische Universität München

Oxidkeramik J Cardenas GmbH (2015). *Material data sheet*. Albershausen

Peng, B., Zhang, H., Shao, H., Xu, Y., Zahng, X., & Zhu, H. (2016). Thermal conductivity of monolayer MoS2, MoSe2 and WS2: interplay of mass effect, interatomic bonding and anharmonicity. *RSC Advances*. 6,5767-5773.

Reitschuster, S., Maier, E., Lohner, T., & Stahl, K. (2020). Friction and temperature behavior of lubricated thermoplastic polymer contacts. *Lubricants*, *8*, 67.

Ronkainen, H., Varjus, S., & Holmberg, K. (1998). Friction and wear properties in dry, water- and oil-lubricated DLC against alumina and DLC against steel contacts. *Wear*, *222*, 120–128.

Schouten, M. J. M. (1973). *The influence of elastohydrodynamic lubrication on friction, wear and durability of gears (in German)*. Dissertation, University of Eindhoven

Schul, C. (1997). *Einfluß der Baugröße auf die Lebensdauer feststoffgeschmierter Kugellager*. Dissertation, Technische Universität Darmstadt

Schultrich, B., & Weihnacht, V. (2008). Tribological behavior of hard and super hard carbon layers. *Vakuum in Forschung und Praxis*, 20,12–17 (in German).

Stößel, K. (1971). *Coefficients of friction under elasto-hydrodynamic conditions (in German)*. Dissertation, Technische Universität München

Tsai, F., Blanton, T., Harding, D. R., & Chen, S. (2003). Temperature dependence of properties of vapor deposited polyimide. *Journal of Applied Physics*, *93*, 3760–3764.

Vazirisereshk, M. R., Martini, A., Strubbe, D. A., & Baykara, M. Z. (2019). Solid lubrication with MoS2: a review. *Lubricants*. 7,57.

Weihnacht, V., Makowski, S., Brückner, A., Theiler, G., & Gradt, T. (2012). Tribology and applications of ta-C layers under dry lubrication. *Tribologie und Schmierungstechnik* (in German). 59(6),41-44.

Xu, J., Zhu, M. H., Zhou, Z. R., Kapsa, P., & Vincent, L. (2003). An investigation on fretting wear life of bonded MoS2 solid lubricant coatings in complex conditions. *Wear*, *255*, 253–258.

Yilmaz, M., Kratzer, D., Lohner, T., Michaelis, K., & Stahl, K. (2018). A study on highly-loaded contacts under dry lubrication for gear applications. *Tribology International*, *128*, 410–420.

Yukhno, T. P., Vvedenskij, Y. V., & Sentyurikhina, L. N. (2001). Low temperature investigations on frictional behavior and wear resistance of solid lubricant coatings. *Tribology International*, *34*, 293–298.

Zhang, H. J., Zhang, Z. Z., & Guo, F. (2011). Studies on the influence of graphite and MoS2 on the tribological behaviors of hybrid PTFE/Nomex fabric composite. *Tribology Transactions*, *54*(3), 417–423. https://doi.org/10.1080/10402004.2011.553027.

Ziegltrum, A., Maier, E., Lohner, T., & Stahl, K. (2020). A numerical study on thermal elastohydrodynamic lubrication of coated polymers. *Tribology Letters*, *68*(2). https://doi.org/10.1007/s11249-020-01309-6.

Publisher's Note